Effects of terrigenic He components on tritium–helium dating: A case study of shallow groundwater in the Saijo Basin

Yasunori Mahara[a,b*], Tomoko Ohta[b], Noritoshi Morikawa[c], Takanori Nakano[d], Minoru Tokumasu[e], Satoshi Hukutani[f], Tomochika Tokunaga[g] and Toshifumi Igarashi[b]

[a] Kyoto University, Kyoto 606-8501, Japan,

[b] Graduate School of Engineering, Hokkaido University, Sapporo 060-8626, Japan,

[c] Advanced Industrial Science and Technology, Tsukuba 305-8561, Japan,

[d] Research Institute for Humanity and Nature, Kyoto 603-8047, Japan,

[e] Saijo Municipal Office, Saijo 793-8601, Japan,

[f] Research Reactor Institute, Kyoto University, Kumatori 590-0494, Japan.

[g] Department of Environmental Systems, School of Frontier Sciences, University of Tokyo, Kashiwa, 277-8563, Japan.

* Corresponding author: mahara@mta.biglobe.ne.jp

Abstract

Dating using a combination of ^{3}H and ^{3}He is believed to be the most practical method for estimating the short residence time of shallow groundwater. However, this method must estimate tritiogenic ^{3}He alone and tends to overestimate the residence time of groundwater, if terrigenic ^{3}He from the mantle cannot be excluded from the total dissolved ^{3}He. We demonstrate the exclusion of terrigenic ^{3}He in the Saijo Basin, where mantle He is easily released along the major active fault, Median Tectonic Line. The $^{3}He/^{4}He$ ratios suggest that the west bank of the Kamo River, which lies within the basin, has experienced greater emanations of mantle He than the east bank. We estimate the residence times to be 1.1–96 years by the proposed exclusion method.

1. Introduction

Groundwater is one of most indispensable water resources for human activities. As the overuse of groundwater leads to exhaustion, adequate management based on the residence time of groundwater is required to regulate its use. Dating using a combination of ^{3}H and ^{3}He is believed to be the most practical method for estimating the short residence time of shallow groundwater (Solomon et al., 1993; Aeschbach-Herting et al., 1998, 1999; Solomon and Cook, 2000; Kipfer et al., 2002). The residence time (T) of groundwater is estimated by the following equation:

$$T = 17.69 \ln [4.01 \times (^{3}He_{tri})/(HTO) \times 10^{14} + 1], \quad (1)$$

where T is the residence time of groundwater (years), $^{3}He_{tri}$ is the accumulated tritiogenic ^{3}He produced through β decay of ^{3}H in groundwater (ccSTP/g $_{water}$), and HTO is the tritium concentration in groundwater (TU).

However, as this method is based on the estimation of only tritiogenic ^{3}He produced through β decay of ^{3}H (Mahara and Ohta, 2009), the residence time of groundwater tends to be overestimated if the addition of terrigenic ^{3}He (i.e. mantle ^{3}He supplied from depth and radiogenic ^{3}He from the crust) is not appropriately considered. If mantle He is released into shallow groundwater, the contribution of ^{3}He that originated in mantle He is greater than that from radiogenic He. Mantle He exhibits $^{3}He/^{4}He$ ratios of 1.1×10^{-5}

in subduction areas, including Japan (Sano and Wakita, 1985), whereas radiogenic $^{3}He/^{4}He$ ratios are typically around 1×10^{-8} (Porcelli et al., 2002). Furthermore, mantle ^{3}He released along the volcanic fronts and major active faults of Japan can be easily monitored (Fig. 1), and most Japanese groundwater has been affected by mantle ^{3}He supplied from the depths.

This study proposes a method that incorporates the rest of the ^{3}H, which has not yet decayed, and the net tritiogenic ^{3}He produced by the β decay of ^{3}H in groundwater after subtracting the accumulation of terrigenic ^{3}He supplied from other sources (e.g., the mantle He) from the total ^{3}He dissolved in groundwater. Then, this study presents an estimation of groundwater residence time in the Saijo Basin, Japan, by the proposed method.

2. Exclusion of terrigenic ^{3}He

The total dissolved ^{3}He concentration $^{3}He_{(Tot)}$ in groundwater can be expressed as follows:

$$^{3}He_{(Tot)} = {}^{3}He_{(At)} + {}^{3}He_{(Ex.air)} + {}^{3}He_{(Trit)} + {}^{3}He_{(Rad)} + {}^{3}He_{(Mnt)} \qquad (2)$$

where $^{3}He_{(At)}$ represents equilibrated atmospheric ^{3}He at the recharge temperature, salinity, and pressure, $^{3}He_{(Ex.air)}$ represents ^{3}He from excess air (i.e., air entrapped in

groundwater during infiltration in the unsaturated zone), $^{3}He_{(Trit)}$ is derived from β decay of ^{3}H (including natural and man made components), $^{3}He_{(Rad)}$ is derived from β decay of ^{3}H produced through the nuclear reaction of $^{6}Li(n, \alpha)^{3}H$ in crustal rocks, and $^{3}He_{(Mnt)}$ is derived from the release of mantle ^{3}He. Then, the net tritiogenic ^{3}He can be calculated from eq. (1) as follows:

$$^{3}He_{(Trit)} = {}^{3}He_{(Tot)} - {}^{3}He_{(At)} - {}^{3}He_{(Ex.air)} - {}^{3}He_{(Rad)} - {}^{3}He_{(Mnt)} \qquad (3)$$

We estimate $^{3}He_{(At)}$ and $^{3}He_{(Ex.air)}$ from the recharge temperature of groundwater and excess air effects, which are optimally deduced from the measured correlation between heavy noble gases (Ne, Ar, Kr and Xe) concentrations using the CE-model proposed by Aeschbach-Herting et al. (2000) and iterations. The fourth term $^{3}He_{(Rad)}$ is generally negligible in groundwater with a short residence time because the accumulation rates of $^{3}He_{(Rad)}$ are typically less than 10^{-16} ccSTP/$g_w \cdot y^{-1}$ (i.e., we assumed that the $^{3}He/^{4}He$ ratio for the radiogenic He component is 10^{-8}, and total ^{4}He accumulation rates range from 10^{-8} ccSTP/$g_w \cdot y^{-1}$ to 10^{-12} ccSTP/$g_w \cdot y^{-1}$ for igneous and sedimentary rocks, respectively) and can easily be masked by the fifth term $^{3}He_{(Mnt)}$ if considerable mantle He release is confirmed in the basin. Here we define terrigenic ^{3}He ($^{3}He_{(Terr)}$) which is the sum of mantle ^{3}He and radiogenic ^{3}He. Therefore, we can rewrite eq.(2) as follows:

$$^{3}He_{(Trit)} = {}^{3}He_{(Tot)} - {}^{3}He_{(At)} - {}^{3}He_{(Ex.air)} - {}^{3}He_{(Terr)}. \quad (34)$$

After subtracting from eq. (3) the effects of both the saturated atmospheric $^{3}He_{(At)}$ at the estimated recharge temperature and the re-equilibrated $^{3}He_{(Ex.air)}$ of excess air in groundwater, we can reduce eq. (3) into eq. (4) using the new term $^{3}He^{*}_{(Tot)}$ (= $^{3}He_{(Tot)} - {}^{3}He_{(At)} - {}^{3}He_{(Ex.air)}$) as follows:

$$^{3}He_{(Trit)} = {}^{3}He^{*}_{(Tot)} - {}^{3}He_{(Terr)}. \quad (45)$$

Additionally, we can graphically estimate the magnitude of $^{3}He_{(Terr)}$, as shown in Fig. 2.

In the graph, the total dissolved ^{4}He concentration $^{4}He_{(Sam)}$ and the ^{3}He/^{4}He ratio $R_{(Sam)}$, corrected for both the concentration of ^{4}He and ^{3}He in atmospheric saturation and the excess effects from the air trapped in the sample water, are expressed as a new parameter $x = {}^{4}He_{(S)}/{}^{4}He_{(Sam)}$ ($0 \leq x \leq 1$). This parameter is transformed using the $^{4}He_{(S)}$ concentration saturated with the atmospheric ^{4}He at the estimated recharge temperature under conditions of 1.0 atm and 0‰ salinity, and the corrected $R_{(Sam)} = {}^{3}He^{*}_{(Tot)}/{}^{4}He_{(Sam)}$.

In the next step, we have to estimate the marginal terrigenic ^{3}He/^{4}He ratio accumulated in the groundwater basin. We can estimate the marginal ^{3}He/^{4}He ratio $R_{(Terr)x=0}$ (i.e., it was in secular equilibrium at the end point $x = 0$ on the terrigenic ^{3}He accumulation line) for a certain groundwater flow region. We can draw the terrigenic ^{3}He accumulation line from the starting point ($x = 1.0$, $R_{(Terr)x=1.0} = 0$) to $R_{(Terr)\ x=0}$ =

$R_{(Terr)0}$ at the end point (0, $R_{(Terr)\ 0}$). Using real data, we can estimate the marginal ^{3}He/^{4}He ratio $R_{(Terr)\ 0}$ for x = 0 by extrapolating the terrigenic ^{3}He accumulation line plotting data (x, $R_{(Sam)}$) for samples that are tritium-free and contain a dissolved ^{4}He concentration of more than ten times as much as the atmospheric saturated ^{4}He concentration at the estimated temperature (i.e., $x < 0.1$).

The total ^{3}He dissolved in the sample groundwater is expressed as follows in Fig. 2.

$$^3He^*_{(Tot)} = (^4He_{(S)}/x) \times R_{(Sam)} \qquad (56)$$

Finally, eq. (5) contains both tritiogenic ^{3}He and terrigenic ^{3}He. The net tritiogenic ^{3}He in the sample water can be calculated by subtracting $R_{(Terr)x}$ on the terrigenic ^{3}He accumulation line from $R_{(Sam)}$ for the sample as follows:

$$^3He_{(Trit)} = (^4He_{(S)}/x)\cdot(R_{(Sam)x} - R_{(Terr)x}) \qquad (67)$$

We can determine $R_{(Terr)x}$ on the terrigenic ^{3}He accumulation line by eq. (7), which connects two points (0, $R_{(Terr)\ 0}$) and $(1.0, 0)$:

$$R_{(Terr)x} = R_{(Terr)\ 0} \times (-x + 1)(0 \le x \le 1.0) \qquad (78)$$

In our proposed method, we assume that terrigenic ^{3}He constantly accumulates in groundwater without diffusing and degassing. This is because diffusion and degassing effects are negligible during the short residence time of groundwater in a shallow aquifer owing to small diffusion coefficients of ^{3}He (e.g., 6.3×10^{-3} m^2/a in sedimentary

rock (Osenbrück at al., 1998) and 4.7×10^{-2} m^2/a in a recharged zone in a silty sand aquifer with an effective porosity of 30% (Solomon and Cook, 2000)) and containing a low ^4He concentration and low volatile gases.

3. Geological setting of the study area

Figure 1 illustrates the plate tectonic setting around the Japanese Islands and indicates the location of two volcanic fronts, a major active fault, i.e., the Median Tectonic Line (MTL), the Japan Trench, and the Nankai and Okinawa troughs. The formation of Shikoku Island, including the Saijo Basin, was extensively affected by subduction of the Philippine Sea plate beneath the Eurasian plate. This subduction resulted in the formation of the Nankai Trough and led to the storage of a large volume of accretionary prism material in the Shikoku forearc basin. Broadly, Shikoku Island can be divided into two major geological zones along the MTL: the Inner Zone facing the Setouchi Sea and the Outer Zone facing the Pacific Ocean. The Outer Zone was formed by the loading of three major accretionary prisms namely the Sambagawa metamorphic belt, the Chichibu belt, and the Shimanto belt. The Inner Zone consists of the Late Cretaceous Ryoke Granite, the metamorphic rocks of the Jurassic accretionary complex, and the Izumi Group, which consists of thick marine sedimentary rocks of Late

Cretaceous age (Fig. 3).

The Saijo Basin is located at the southern edge of the Inner Zone and is in contact with the Outer Zone along the MTL. The basin is buried by thick alluvial deposits, which formed fans at the mouths of rivers crossing the MTL. Many artesian springs are observed beyond the alluvial fan (Fig. 3). The basin is divided by the Kamo River to form its east and west banks, and the west bank is underlain by the Ryoke Granite. Conversely, the granite exists at depth on the east bank, with the Izumi Group overlying it. Both banks have been reclaimed inland for some kilometers from the Setouchi Sea shore line over the past few hundred years.

Figure 3 shows the positions of two vertical sections along line A–A' on the west bank and line B–B' on the east bank, and Fig. 4 illustrates the shallow groundwater aquifer structures in these two vertical sections. Both aquifers include an upper unconfined aquifer (which consists of sand and pebbles) to a depth of −10 m and a lower confined aquifer (which consists of sand overlying clay, silt, and pebbles) to a depth of −40 m. The upper and lower aquifers are divided by an impermeable layer, which consists of clay and silt and is thick on the west bank and thin on the east bank. At some places, this impermeable layer disappears near the edge of the mountainous area on the east bank.

The Saijo Basin is rich in groundwater with a recharge zone located at a back mountainous area. The highest peak surrounding the basin is Mt. Ishizuchi, which retains traces of Tertiary volcanism. If we assume that mantle He is easily released along many veiled or unveiled faults, including the MTL, that are present along the edge of the mountainous area, we cannot rule out the possibility that terrigenic ^{3}He is added during groundwater discharge to the Setouchi Sea.

4. Materials and methods

4.1 Sampling of groundwater

Eighteen groundwater samples were collected from the wells listed in Fig. 3 and Table 1. The first and second sampling campaigns were conducted during July 15–17, 2008 and December 25–26, 2012, respectively. Eleven samples were collected from artesian wells. Sample 1 (Kanpusan) was collected from seepage flow at high altitude; samples 3 and 17 (Minato Shinchi), 8 (Omachi P-school), 14 (Kobhosui), 15 (Hiuchi hot spa), and 18 (Kurare) were collected from pumping water. We collected sample 15 to confirm whether mantle He has been marginally released at depth on the east bank of the Kamo River.

Groundwater samples were collected for measurement of the concentrations of ^{3}H and dissolved noble gases. The volumes of the water samples were 1000 mL and 15 mL

for ^{3}H and dissolved noble gas concentrations, respectively. The samples were carefully collected under pumping conditions or natural flow conditions. Furthermore, the samples analyzed for dissolved noble gas contents were collected in annealed Cu tubes; both ends of the Cu tubes were pinched off with steel clamps to prevent the dissolved gases from degassing or becoming contaminated with atmospheric air during long-term storage.

4.2 Analytical methods

The concentration of tritium (HTO) was measured by β-ray counting after electrolytic enrichment, and 1 L of groundwater was reduced to approximately 40 mL by electrolysis using Ni/Fe electrodes. 40 mL of distillate and 60 mL of scintillation cocktail (Aquaso-II, New England Nuclear Ltd.) were mixed in a 100-ml Teflon vial. This mixture was measured for 1000 min using a low-background liquid scintillation counter. The detection limit of tritium was 0.03 Bq/L (0.25 TU).

Following the exclusion of moisture and other gases (except noble gases) using a cold trap and a heated Ti–Zr getter (800 °C), each noble gas component was separated by cooling in a charcoal trap with liquid nitrogen using a cryogenic pump equipped with a sintered stainless steel trap (Nagao et al., 2010). Then, a VG5400(MS-III) noble gas

mass spectrometer was used to measure the concentration of dissolved ^{4}He (with a measurement error of 1%), the $^{3}He/^{4}He$ ratio (with a standard deviation of 1σ at less than 5% for at least 50 iterations), the concentration of ^{20}Ne, the $^{22}Ne/^{20}Ne$ ratio, the concentration of ^{40}Ar, the $^{36}Ar/^{40}Ar$ ratio, the concentration of ^{84}Kr, and the concentration of ^{132}Xe. ^{20}Ne and ^{22}Ne measurements were corrected for $^{40}Ar^{+}$ and CO_2^{+} before and after Ne analysis (Nagao et al., 2010). According to Nagao et al. (2010), the contributions of $^{40}Ar^{2+}$ and CO_2^{2+} to $^{20}Ne^{+}$ and $^{22}Ne^{+}$ are as low as <0.4% and <0.01%, respectively. The total experimental uncertainties for noble gas concentrations were estimated to be 10%, which is based on the reproducibility of measurements for a standard gas and ambiguities in the gas reduction procedure (Kotarba and Nagao, 2008).

In this study, the $^{3}He/^{4}He$ ratio for standard air was assumed to be 1.4×10^{-6} (Ozima and Podosek, 1983). The average stripping efficiency of dissolved gases from the sample water, based on the reproducible measurements, was determined to be 97% of that of ^{4}He and ^{20}Ne in samples of distilled water equilibrated with atmospheric air at 23 °C. We corrected the dissolved concentrations of ^{4}He and ^{20}Ne using this extracted efficiency (Table 1).

5. Results

Table 1 presents the measured dissolved noble gases and tritium concentrations in groundwater, estimates of the effects of excess air and recharge temperature using the CE-model, and the residence times estimated using the new dating methods proposed in this study (i.e., by combining the measured concentration of ^{3}H with the net ingrown tritiogenic ^{3}He alone estimated in eq. (4) and excluding terrigenic ^{3}He from the rest of ^{3}He ($^{3}He^{*}_{(Tot)}$) by subtracting both the atmospheric equilibrated ^{3}He and the re-equilibrated ^{3}He in the partial dissolution of excess air). The dissolved ^{4}He concentrations range from 4.32×10^{-8} ccSTP/g to 4.56×10^{-7} ccSTP/g, with the exception of samples 11, 12, and 15 in which the concentrations range from the saturated concentration of atmospheric ^{4}He to ten times its value. The concentrations of samples 11, 12, and 15 are approximately 80 times the saturation concentration of atmospheric ^{4}He, and the slightly high $^{3}He/^{4}He$ ratios of samples 11 and 12 ($>2.5 \times 10^{-6}$) suggest the accumulation of a mantle He component. Conversely, the slightly low $^{3}He/^{4}He$ ratio (10^{-7}) of sample 15 suggests an accumulated radiogenic He component.

All samples except samples 11 and 12 contain excess air judging from the correlation between the $^{20}Ne/^{36}Ar$ ratio and the ^{20}Ne concentration in Fig. 5. Samples 11 and 12 were degassed but retained large amounts of dissolved ^{4}He. We showed the corrected ^{4}He concentration using the diffusion model (Stute et al., 1992) based on the differences

between the diffusion coefficients of He and Ne and estimates of the isotopic fractionation between ^{3}He and ^{4}He. This method is based on an analogous method for estimating isotopic fractionation under conditions of non-equilibrium degassing (Lippmann et al., 2003), at a groundwater sampling temperature of 8 °C. The tritium concentrations of the other samples, except samples 3, 12, 15, and 17, exceed the detection limit of 0.25 TU and range from 0.6 TU to 3.3 TU. However, the tritium concentrations of samples 3, 12, 15, and 17 were less than the detection limit. Furthermore, samples 3 and 17 were obtained from the same well in the shallow aquifer, although they were collected 4 years apart during different sampling campaigns. Sample 11 was collected from the deep aquifer at its contact with the MTL, and sample 15 was collected at a depth of −1005 m from a well drilled in the thick alluvium.

6. Discussion

6.1 Emanation of mantle ^{3}He in the Saijo Basin

Figure 6 illustrates the correlation between the ratios R ($^{3}He/^{4}He$) and x for all groundwater samples and for the Ishizuchi hot spa (Fig. 3), for which Dogăn et al. (2006) reported the highest ratio on Shikoku Island (4.98×10^{-6}). R in the present study is also high ($4.71 \pm 0.05 \times 10^{-6}$), with a dissolved ^{4}He concentration of 9.36×10^{-7}

ccSTP/g at the hot spa. As the Ishizuchi hot spa is located close to Mt. Ishizuchi, which is a Tertiary volcano, we assume that a certain amount of mantle He has been added to the hot spring water. Although Quaternary volcanism on Shikoku Island remains unconfirmed, a relatively high *R* ratio has been observed in many groundwater and hot spring samples along the major active fault, i.e., the MTL (Dogăn et al., 2006). These observations suggest that mantle He with a high *R* ratio is easily released into groundwater from deep underground through classified and unclassified faults.

All samples in the present study can be allocated to one of the two groundwater groups, namely the east and west banks of the Kamo River. Samples collected from the west bank exhibit higher *R* ratios ($1.49–2.83 \times 10^{-6}$) than those from the east bank ($0.65–2.02 \times 10^{-6}$). Furthermore, samples 11 and 12, which were collected from the west bank, have significantly higher He concentrations ($3.5–3.75 \times 10^{-6}$ ccSTP/g) and *R* ratios ($2.58–2.68 \times 10^{-6}$) than the other samples. These results suggest that a mantle He component was actively transported along faults from depth, particularly because the hot spas are located above or in the vicinity of the MTL. Conversely, most shallow groundwater samples collected from the east bank (except sample 15) exhibit low He contents ($4.32–45.6 \times 10^{-8}$ ccSTP/g) and *R* ratios ($1.37–2.02 \times 10^{-6}$) compared to those from the west bank. We exclude sample 15 (Hiuchi hot spa) from the shallow

groundwater group on the east bank, as this sample was collected from a depth of −1005 m and does not exhibit a clear relationship with the shallow groundwater group (i.e., those above −60 m) discussed here, because of considerable accumulation of radiogenic He.

If the dissolved He characteristics of sample 15 (atmospheric He: 1.2 %, mantle He: 5.5 %, radiogenic He: 93.3 %) are representative of the deep groundwater in the east bank area, the mantle He component must have contributed less than 6% of the total dissolved He concentration, according to estimations of the mixing rate obtained by the three-He-component mixing model (Sano and Wakita, 1985, 1988) among the atmospheric He component (R: 1.36×10^{-6}, the equilibrated $^{20}Ne/^{4}He$ ratio: 3.86 at the estimated recharge temperature), radiogenic He (R: 1×10^{-8}, the $^{20}Ne/^{4}He$ ratio:10^{-3}), and mantle He (R: 1.1×10^{-5}, the $^{20}Ne/^{4}He$ ratio: 10^{-3}) in groundwater. Conversely, if samples 11 (atmospheric He: 0.9 %, mantle He: 23.7 %, radiogenic He: 75.3 %) and 12 (atmospheric He: 0.8 %, mantle He: 24.8 %, radiogenic He: 74.4 %) are representative of the dissolved He characteristics of deep groundwater for the west bank, mantle He must have contributed 24% of the total He as per the aforementioned mixing model.

6.2 Accumulation of terrigenic He in shallow groundwater in the Saijo Basin

We must first rescale the correlation between $x = {}^4He_{(S)}/{}^4He_{(Sam)}$ and $R_{(Sam)} = {}^3He^*_{(Tot)}/{}^4He_{(Sam)}$ and check the characteristics of He accumulated in groundwater to exclude the effects of the terrigenic He accumulation as shown in Fig. 2, after correcting for the effects of the dissolved atmospheric air and the excess air or degassing. In the east bank area, we determined the accumulated He characteristics for the discharged groundwater by extrapolating the terrigenic ^3He accumulation line ($R_{(Terr)x} = R_{(Terr)0} \times (-x + 1)\ (0 \leq x \leq 1.0)$) passing through samples 3 and 17 from the starting point of x = 1.0 to the end point of x = 0, as shown in Fig. 7. We selected the average point between samples 3 and 17 as the passing point because the tritium content in these samples was lower than the detection limit (0.25 TU) and exhibited the highest concentrations of ^4He in the east bank area (Table 1). The estimated marginal $R_{(Terr)0}$ (at x = 0) was 1.48×10^{-6} from the intercept at x = 0 on the terrigenic ^3He accumulation line (i.e., $R_{(Terr)x} = 1.48 \times 10^{-6} \times (-x+1)$). Therefore, the marginal $R_{(Terr)0}$ for the terrigenic He component was estimated including a mantle He contribution of 13% from the aforementioned mixing model (Sano and Wakita, 1985, 1988); this would have gradually accumulated in shallow groundwater such that its concentration would have increased with increasing residence time.

In the west bank area, sample 11 ($R = 2.63 \times 10^{-6}$, i.e. corrected degassing effects

shown in Table 1) was the only sample under the detection limit of tritium and contained abundant ^{4}He (x = 9.03 × 10^{-3}), as shown in Table 1, after correcting for degassing effects. We used this sample to determine marginal $R_{(Terr)0}$ of the terrigenic ^{3}He accumulated in groundwater. Although sample 11 is located close to the recharge zone, the He component that is rich in mantle He in the sample is actively supplied from a depth. Therefore, the terrigenic ^{3}He readily accumulates in groundwater along the MTL and other unclassified faults in the west bank area. We adopted the ratio of sample 11 (2.63 × 10^{-6}) such that the marginal $R_{(Terr)0}$ of the terrigenic ^{3}He accumulated in groundwater is 2.65 × 10^{-6} (Fig. 7). Consequently, the terrigenic ^{3}He with marginal $R_{(Terr)0}$ = 2.65 × 10^{-6} (including a 24% contribution from mantle He) must have gradually accumulated in the shallow groundwater on the terrigenic ^{3}He accumulation line ($R_{(Terr)x}$ = 2.65 × 10^{-6} × $(-x + 1)$) with increasing residence time. In conclusion, the groundwater in the west bank area is twice as rich in terrigenic ^{3}He as that in the east bank area.

6.3 Estimates of residence times of shallow groundwater in the Saijo Basin

Uncertainties in estimates of residence time are introduced by several factors: measurement of noble gases; corrections related to degassing processes, excess air, and

recharge temperature; and determination of the terrigenic ^{3}He accumulation line. However, we can control uncertainties in corrections related to degassing processes, excess air, and recharge temperature by the method of minimizing “the sum of the weighted squared deviations σ_i between the estimate in models and measured concentrations of heavy noble gases (Ne, Ar, Kr and Xe)” in eq. (12), cited after Aeschbach-Herting et al. (1999). We used 10% as $1\sigma_{i,}$ taking into consideration a total experimental error of 10% for the reproducibility of measurements for a standard gas and ambiguities in the gas reduction procedures for measurement of noble gases in samples.

The uncertainty in the determination of the terrigenic ^{3}He accumulation line is greater than other uncertainties in this study, because the characteristics of He released in the basin were deduced from a very limited number of samples. When we drew the terrigenic ^{3}He accumulation line using groundwater samples 3 and 17 collected from the same well at different sampling dates in the discharged zone of the east bank, changes in the $^{3}He/^{4}He$ ratio, the dissolved ^{4}He concentration, the excess air content, and the recharged temperature were not significant over 4 years. Therefore, uncertainties in the east bank area may be small if groundwater samples 3 and 17 can be considered to represent the discharge zone. On the other hand, in the west bank area, we drew the

terrigenic ^{3}He accumulated line using only sample 11, which we assumed to be representative groundwater in the discharge zone although being slightly degassed. For discussion on the representation of sample 11, we have to intensively survey groundwater in which the tritium concentration is less than the detection limit and both the ^{4}He content and the $^{3}He/^{4}He$ ratio are high; furthermore, we have to specifically investigate the spreading mechanism of the mantle He released through faults in the basin. Although evaluating the uncertainty in the residence time of groundwater estimated by applying our proposed method proved to be difficult, we concluded that the estimates of residence time include at least 10% uncertainty, considering the noble gas experimental error.

We summarized the estimated residence times of all groundwater samples except 2, 3, 11, 15, and 17 according to the proposed method in Table 1. As the tritium concentrations of samples 3, 11, 15, and 17 were less than the detection limits, these samples were not suitable for estimates of residence time using the proposed method for tritium and tritiogenic ^{3}He dating. On the other hand, the residence time could not be estimated for sample 2 because the correction for excess air failed as a result of the ^{4}He content being too low to achieve a suitable relation between r concentrations of ^{20}Ne and ^{40}Ar and the estimated recharged temperature. The final corrected tritiogenic ^{3}He

concentration had a negative value. However, the estimated groundwater residence times for the other samples have a reasonable range of 1.1–96 (a mean and std: 26.4 ± 27.3) years. Nevertheless, groundwater in the Saijo Basin has accumulated crustal He enriched with a mantle He component. The estimated residence times (43.1 ± 10.4years) were reasonably longer in the discharged zone close to the seashore than those (9.5 ± 7.6 years) in the area close to the recharged area of the alluvial fan and underflow zone of the Kamo River (Fig. 3). Sample 12, which is located above the active fault (the MTL), has the longest residence time of 96 years, although we cannot completely exclude effects from deep groundwater gushing out along the fault. Consequently, the proposed method, excluding the mantle ^{3}He, is available for estimates of short residence time in the shallow groundwater. Nevertheless, the basin is loaded with abundant terrigenic ^{3}He that originated from mantle He.

7. Conclusions

(1) The Saijo Basin on Shikoku Island has experienced active accumulation of mantle He, which was released from a depth along a major active fault (MTL) and other faults. The west bank of the Kamo River (where the mantle He component constitutes 24% of the total dissolved He in groundwater) has approximately received twice as much

mantle He as the east bank (where the mantle He component constitutes only 13% of the total dissolved He in groundwater). The estimated residence times obtained for shallow groundwater from our newly proposed method (which excludes terrigenic ^{3}He effects from the total ^{3}He content) range from 1.1 years to 96 years.

(2) We plotted the relationship between $x = {}^4He_{(S)}/{}^4He_{(Sam)}$ and $R_{(Sam)} = {}^3He^*_{(Tot)}/{}^4He_{(Sam)}$ for all samples and proposed a graphical method to determine the characteristics of the terrigenic ^{3}He controlling He accumulation in the basin, after subtracting the dissolved atmospheric ^{3}He and correcting for the excess air using the CE model. The marginal $R_{(Terr)x=0}$ was determined by extrapolation of a straight line passing through selected candidate data that showed high ^{4}He content and was below the tritium detection limit to connect the starting point ($R_{(Terr)x=1} = 0$). In the east bank area, the extrapolated marginal $R_{(Terr)x=0}$ ratio was estimated to be 1.48×10^{-6} on the basis of the intercept at $x = 0$ on the terrigenic ^{3}He accumulation line $R_{(Terr)x} = 1.48 \times 10^{-6} \times (-x + 1)$. For the west bank, the extrapolated marginal $R_{(Terr)x=0}$ ratio was estimated to be 2.65×10^{-6} on the basis of the intercept at $x = 0$ on the terrigenic ^{3}He accumulation line $R_{(Terr)x} = 2.65 \times 10^{-6} \times (-x + 1)$.

(3) The method proposed for the exclusion of terrigenic ^{3}He has proven very useful for evaluating only net tritiogenic ^{3}He ingrown in groundwater, such as in the Saijo Basin

where mantle He has constantly been added from depth. A more precise ^{3}He accumulation line is required for more reasonable estimation of groundwater residence time; this could be achieved by a more thorough investigation of the basin's noble gas hydrology and by reduction of experimental error of noble gas measurements.

References

Aeschbach-Herting W., Schlosser P., Stute M., Simpson H. J., Ludin A., Clark J. F. 1998. A $^{3}H/^{3}He$ study of ground-water flow in a fractured bedrock aquifer. Ground Water. **36**, 661-670.

Aeschbach-Herting W., Peeters F., Beyerle U., Kipfer R., 1999. Interpretation of dissolved atmospheric noble gases in natural waters. Water Resour. Res., **35**, 2779-2792.

Aeschbach-Herting W., Peeters F., Beyerle U., Kipfer R., 2000. Palaeotemperature reconstruction from noble gases in ground water taking into account equilibration with entrapped air. Nature, **405**, 1040-1044.

Dogăn, T., Sumino, H., Nagao, K., Notsu, K., 2006. Release of mantle helium from

forearc region of the southwest Japan arc. Chem. Geol. 233, 235–248.

Kipfer, R., Aeschbach-Hertig, W., Peeters, F., Stue, M., 2002. 14. Noble Gases in lakes and ground waters. In Rev. Mineral. Geochem., vol. 47, Noble Gases in Geochemistry and Cosmochemistry, 615–700. DOI:10.2138/rmg.2002.47.14

Kotarba, M. and Nagao, K., 2008. Composition and origin of natural gases accumulation in the Polish and Ukrainian parts of the Carpathian region: Gaseous hydrocarbon, noble gases, carbon dioxide and nitrogen. Chem. Geol. **255**, 426–438.

Lippmann, J., Stute, M., Moser, D.P., Hall, J.A., Lin, L., Borcsik, M., Bellamy, R.E. S., Onstott, T.C., 2003. Dating ultra-deep mine water with noble gases and ^{36}Cl, Witwatersrand Basin, South Africa. Geochim. Cosmochim. Acta **67**, 4597–4619.

Mahara Y., Ohta T., 2009. Groundwater dating by the tritium and helium-3 method and its application. J. Plasma Fusion Res., **85**, 434-436. (in Japanese)

Nagao, K., Kusakabe, M., Yoshida, Y., Tanyileke, G., 2010. Noble gases in Lake Nyos

and Monoun, Cameroon. Geochem. J. **44**, 519–543.

Osenbrück K., Lippmann J., Sonntang Ch, 1998. Dating very old pore waters in impermeable rocks by noble gas isotopes. Geochim. Cosmchim. Acta **62**,3041-3045.

Ozima, M. and Podosek, F.A., 1983. Noble Gas Geochemistry. Cambridge University Press, Cambridge, 367 pp.

Porcelli, D., Ballentine, C. J., Wieler, R., 2002. 1 An overview of noble gas geochemistry and cosmochemistry. In Rev. Mineral. Geochem. vol. 47, Noble Gases in Geochemistry and Cosmochemistry, 1–19. DOI:10.2138/rmg.2002.47.1

Sano, Y., Wakita, H., 1985. Geographical distribution of 3He/4He ratios in Japan: implications for arc tectonics and incipient magmatism. J. Geophys. Res. **90**, 8728–8741.

Sano Y., Wakita H., 1988. He isotope ratio and heat discharge rate in the Hokkaido Island, Northeast Japan. Geochemical J., **22**, 293-303.

Solomon D. K., Schiff S. L., Poreda R. J., and Clarke W. B., 1993. A validation of the $^{3}H/^{3}He$ method for determining groundwater recharge. Water Resources Research, **29**, 2851-2962.

Solomon D. K. and Cook P. G., 2000. ^{3}H and ^{3}He, in Environmental Tracers In Subsurface Hydrology, (ed) Cook P., and Herczeg A. L., Kluwer Academic Publishers, pp.529.

Stute M., Schlosser P., Clarke J. F. and Broecker W. S., 1992. Paleotemperatures in the southwestern United States derived from noble gases in groundwater. Science, **246**, 1000-1003.

Figure Captions

Fig. 1. Plate tectonic setting of Japan and surrounding areas. Also shown are the locations of the Japan Trench, the Nankai Trough, the Okinawa Trough, and the Median Tectonic Line (MTL). The dark grey solid circle indicates the study area (Saijo Basin). The area enclosed by a dot line indicates three major accretionary prisms (i.e. the Sambagawa metamorphic rock, the Chichibu belt and the Shimanto belt are lined up from north to south).

Fig. 2. Schematic figure showing the correlation between the ratios $R_{(Terr)x}$ and $x = {}^4He_{(S)}/{}^4He_{(Sam)}$, with the location of the sample indicated by the black solid square. The total dissolved ^{3}He ($^3He^*_{(Tot)} = ({}^4He_{(S)}/x) \times R_{(Sam)}$) in the sample is the sum of the net ingrowth of tritiogenic ^{3}He ($^3He_{(Trit)} = ({}^4He_{(S)}/x) \times (R_{(Sam)x} - R_{(Terr)x})$) and the accumulation of terrigenic ^{3}He ($^3He_{(Terr)x} = ({}^4He_{(S)}/x) \times R_{(Terr)x}$). The terrigenic ^{3}He accumulation line ($R_{(Terr)x} = R_{(Terr)0} \times (-x + 1)$, $0 \leq x \leq 1$) is also shown. The open black circle is the location of the accumulated terrigenic ^{3}He/^{4}He ratio of $R_{(Terr)x}$ at x.

Fig. 3. Surface geology around the Saijo Basin, with the locations of the groundwater sampling sites (samples 1–18), the Ishizuchi hot spa, Mt. Ishizuchi, the MTL, the

Kamo River, Artesian Spring Belt and Alluvial Fan. The locations of the vertical sections (A–A' and B–B') presented in Fig. 4 are also shown.

Fig. 4. Structure of the groundwater aquifers (showing the relationship between the unconfined shallow aquifer, the impermeable layer, and the deep confined aquifer) for the vertical sections through lines A–A' and B–B' shown in Fig. 3.

Fig. 5. Correlation between the $^{20}Ne/^{36}Ar$ and dissolved ^{20}Ne concentrations, including the 18 measured samples. Also shown is the boundary between the excess air zone and the degassed zone, related to the ratio of $^{20}Ne/^{36}Ar$ and ^{20}Ne concentrations saturated by atmospheric ^{20}Ne and ^{36}Ar under 1 atm, zero salinity, and temperatures ranging from 0 °C to 30 °C. E and W indicate samples collected at the east bank of the Kamo River, and at the west bank of the Kamo River, respectively.

Fig. 6. Correlation between the measured ratios of $R = {}^{3}He/{}^{4}He$ and $x = {}^{4}He_{(14)}/{}^{4}He_{(Sample)}$. $^{4}He_{(14)}$ is 4.572×10^{-8} ccSTP/g (i.e., the concentration of ^{4}He equilibrated with atmospheric He at an average temperature of 14 °C at Saijo, under 1 atm and zero salinity). $^{4}He_{(Sample)}$ is a raw datum measured ^{4}He concentration in a

sample. Also shown are the locations of samples on the west bank of the Kamo River (open circles and ±1 sigma), samples on the east bank (open squares and ±1 sigma), the Ishizuchi hot spa (open triangle and ±1 sigma), and the Hiuchi hot spa (open inverse triangle and ±1 sigma).

Fig. 7. Correlation between $R_{(Sam)} = {}^{3}He^{*}_{(Tot)}/{}^{4}He_{(Sam)}$ and $x = {}^{4}He_{(S)}/{}^{4}He_{(Sam)}$ and locations of the samples, and the magnitude of net tritiogenic ^{3}He. Two terrigenic ^{3}He accumulation lines: E (black single-dotted line): $R_{(Terr)x} = 1.48 \times 10^{-6} \times (-x + 1)$ and W (black double-dotted line): $R_{(Terr)x} = 2.65 \times 10^{-6} \times (-x + 1)$, $0 \leq x \leq 1.0$ are shown, along with the starting point $x = 0$ (open black circle). Solid black squares are samples collected on the east bank of the Kamo River. Solid black triangles are samples collected on the west bank of the Kamo River. Ingrowth of tritiogenic ^{3}He is indicated.

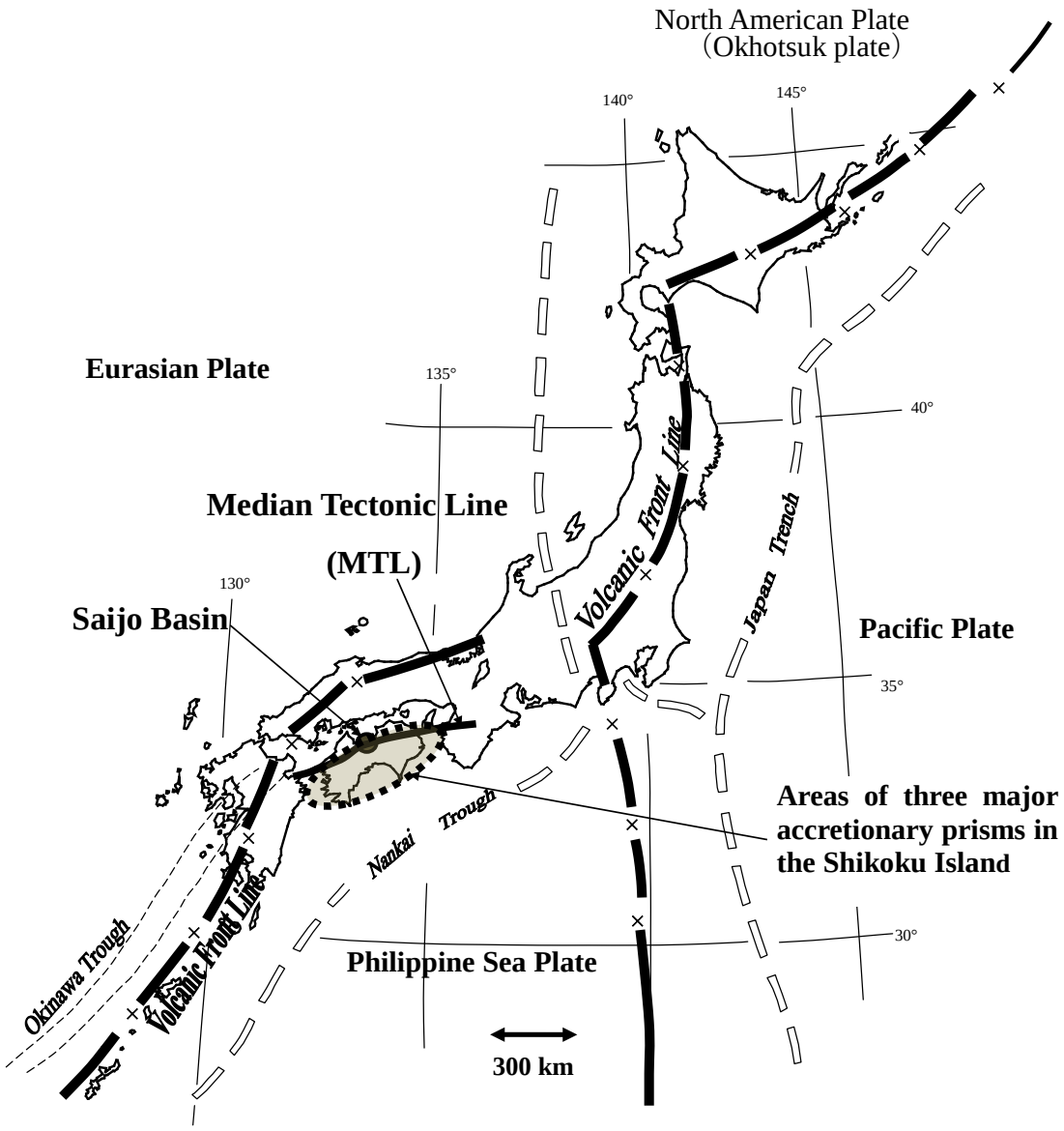
North American Plate
(Okhotsuk plate)
140°
145°
Eurasian Plate
135°
40°
Median Tectonic Line
(MTL)
Volcanic Front Line
Japan Trench
130°
Saijo Basin
Pacific Plate
35°
Areas of three major accretionary prisms in the Shikoku Island
Nankai Trough
Okinawa Trough
Volcanic Front Line
30°
Philippine Sea Plate
300 km

Fig. 1

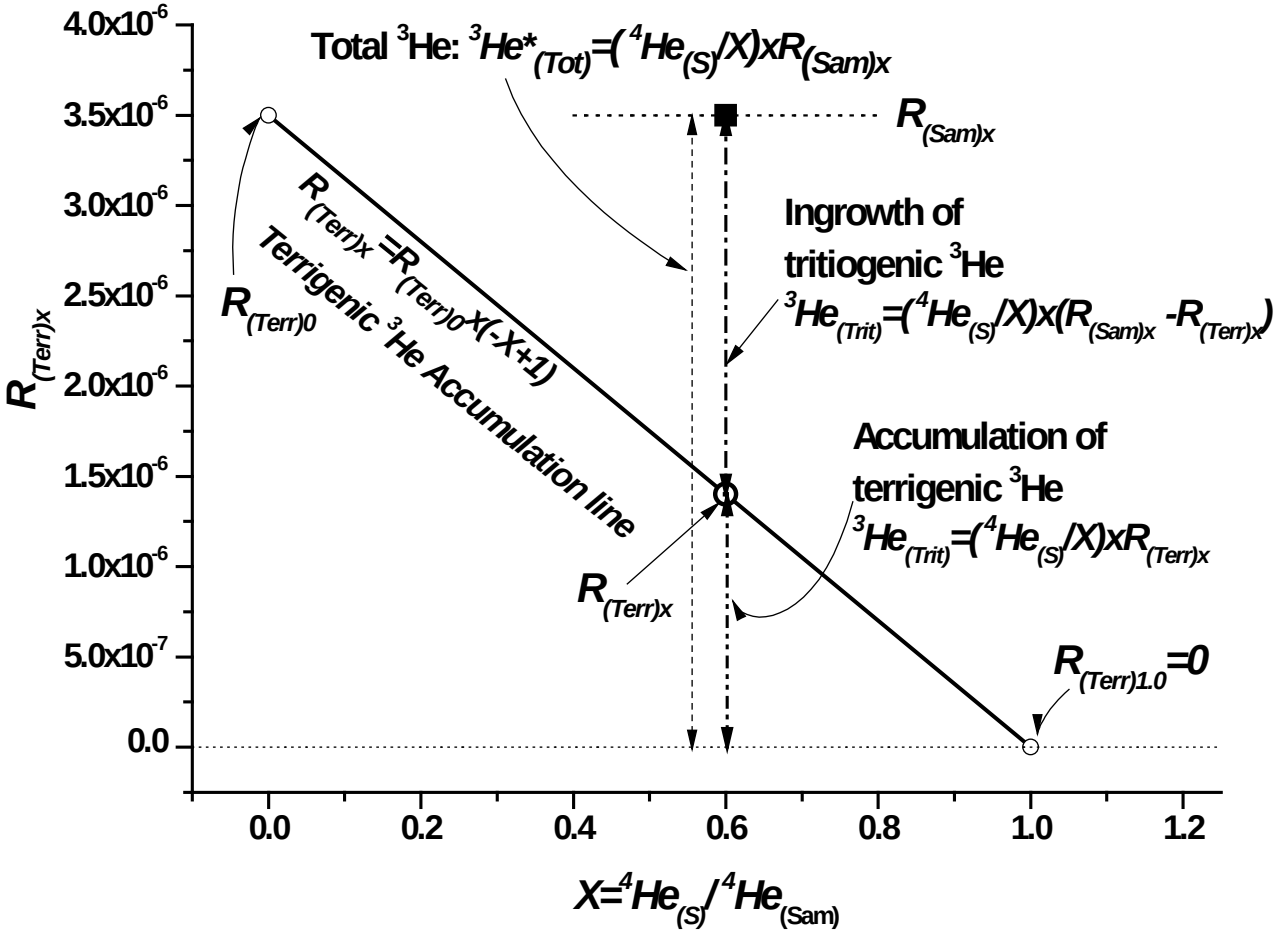
Total ^{3}He: $^3He^*_{(Tot)}=(^4He_{(S)}/X)xR_{(Sam)x}$
$R_{(Sam)x}$
Ingrowth of tritiogenic ^{3}He
$^3He_{(Trit)}=(^4He_{(S)}/X)x(R_{(Sam)x}-R_{(Terr)x})$
$R_{(Terr)x}=R_{(Terr)0}x(-X+1)$
Terrigenic ^{3}He Accumulation line
$R_{(Terr)0}$
Accumulation of terrigenic ^{3}He
$^3He_{(Trit)}=(^4He_{(S)}/X)xR_{(Terr)x}$
$R_{(Terr)x}$
$R_{(Terr)1.0}=0$
$R_{(Terr)x}$
4.0x10^{-6}
3.5x10^{-6}
3.0x10^{-6}
2.5x10^{-6}
2.0x10^{-6}
1.5x10^{-6}
1.0x10^{-6}
5.0x10^{-7}
0.0
0.0
0.2
0.4
0.6
0.8
1.0
1.2
$X=^4He_{(S)}/^4He_{(Sam)}$

Fig. 2

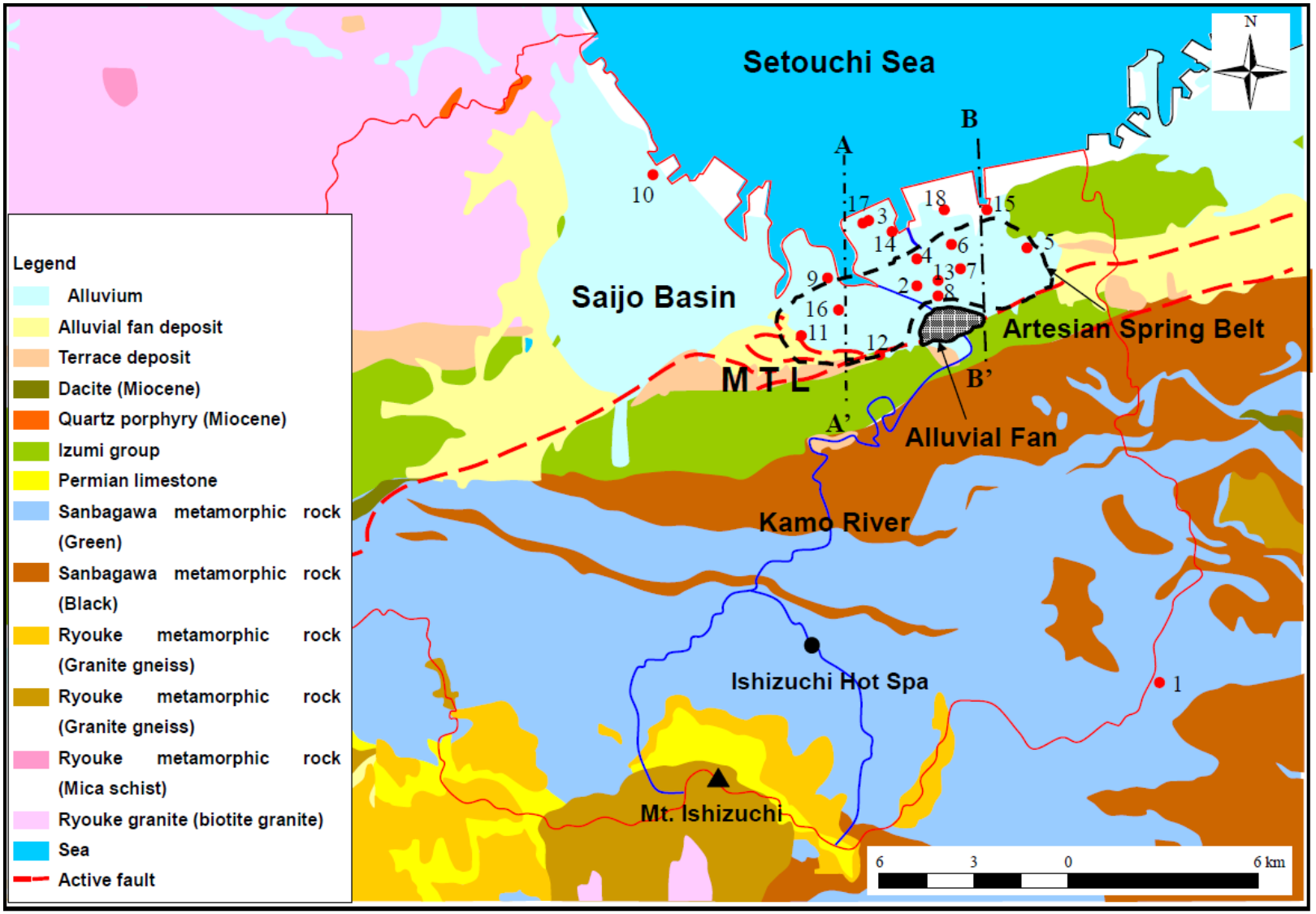
Setouchi Sea
Saijo Basin
Artesian Spring Belt
MTL
Alluvial Fan
Kamo River
Ishizuchi Hot Spa
Mt. Ishizuchi
A
A'
B
B'
N
Legend
Alluvium
Alluvial fan deposit
Terrace deposit
Dacite (Miocene)
Quartz porphyry (Miocene)
Izumi group
Permian limestone
Sanbagawa metamorphic rock (Green)
Sanbagawa metamorphic rock (Black)
Ryouke metamorphic rock (Granite gneiss)
Ryouke metamorphic rock (Granite gneiss)
Ryouke metamorphic rock (Mica schist)
Ryouke granite (biotite granite)
Sea
Active fault
6 3 0 6 km

Fig. 3

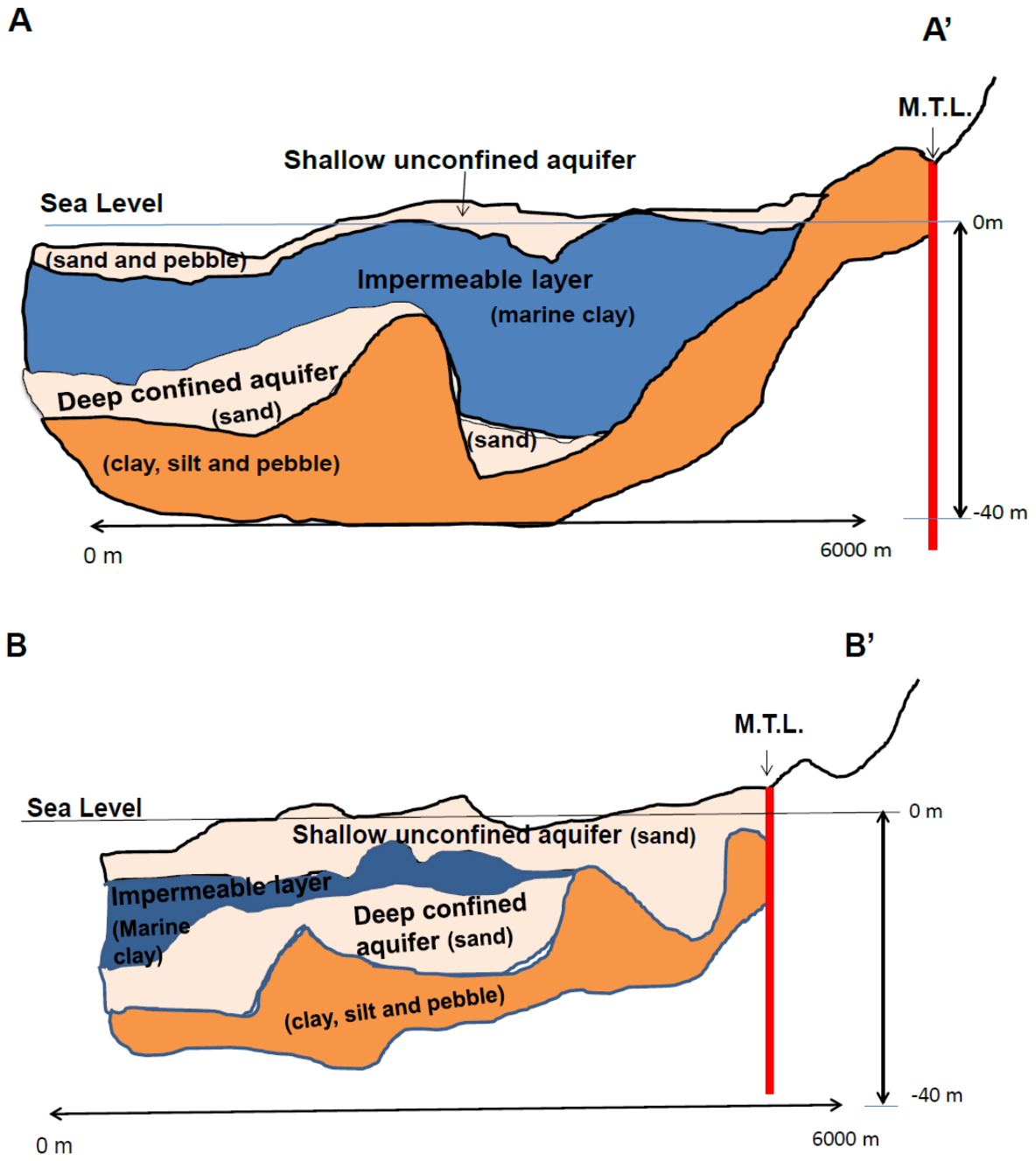
A
A'
M.T.L.
Shallow unconfined aquifer
Sea Level
0m
(sand and pebble)
Impermeable layer
(marine clay)
Deep confined aquifer
(sand)
(sand)
(clay, silt and pebble)
-40 m
0 m
6000 m
B
B'
M.T.L.
Sea Level
0 m
Shallow unconfined aquifer (sand)
Impermeable layer
(Marine clay)
Deep confined aquifer (sand)
(clay, silt and pebble)
-40 m
0 m
6000 m

Fig. 4

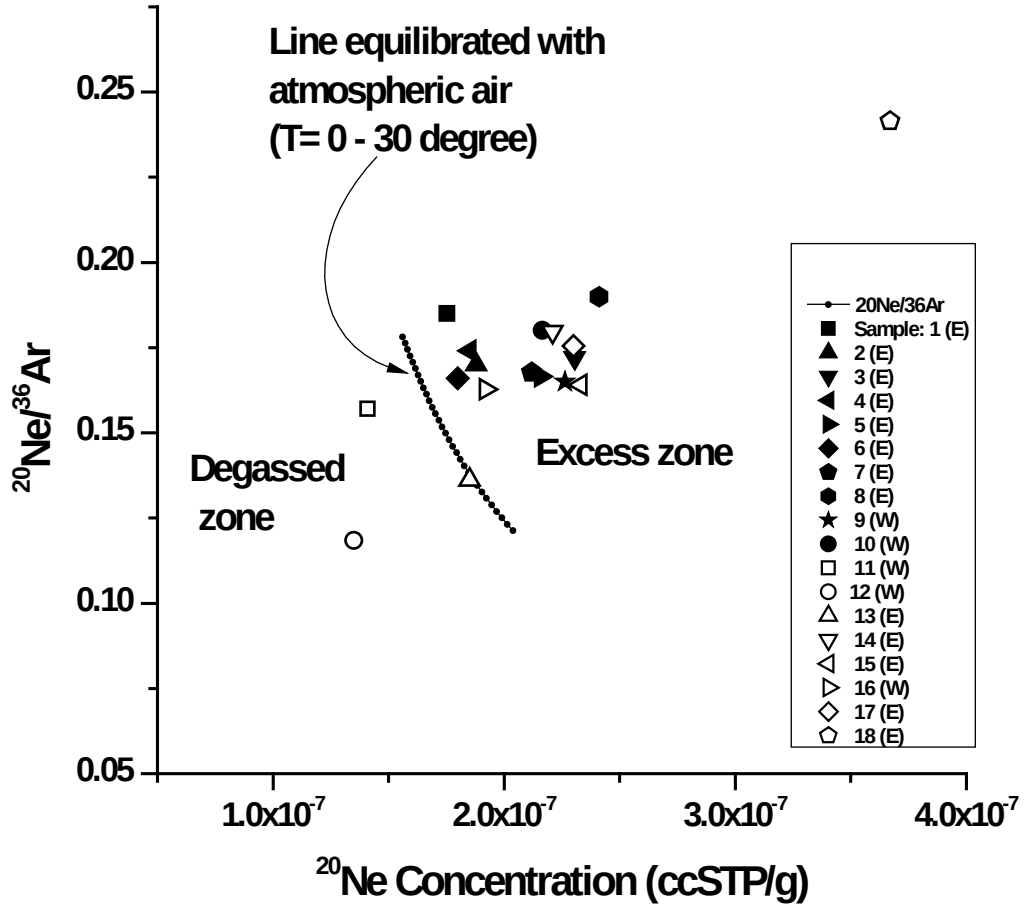
Line equilibrated with
atmospheric air
(T= 0 - 30 degree)
Degassed
zone
Excess zone
0.25
0.20
0.15
0.10
0.05
$^{20}Ne/^{36}Ar$
1.0x10^{-7}
2.0x10^{-7}
3.0x10^{-7}
4.0x10^{-7}
^{20}Ne Concentration (ccSTP/g)
20Ne/36Ar
Sample: 1 (E)
2 (E)
3 (E)
4 (E)
5 (E)
6 (E)
7 (E)
8 (E)
9 (W)
10 (W)
11 (W)
12 (W)
13 (E)
14 (E)
15 (E)
16 (W)
17 (E)
18 (E)

Fig. 5

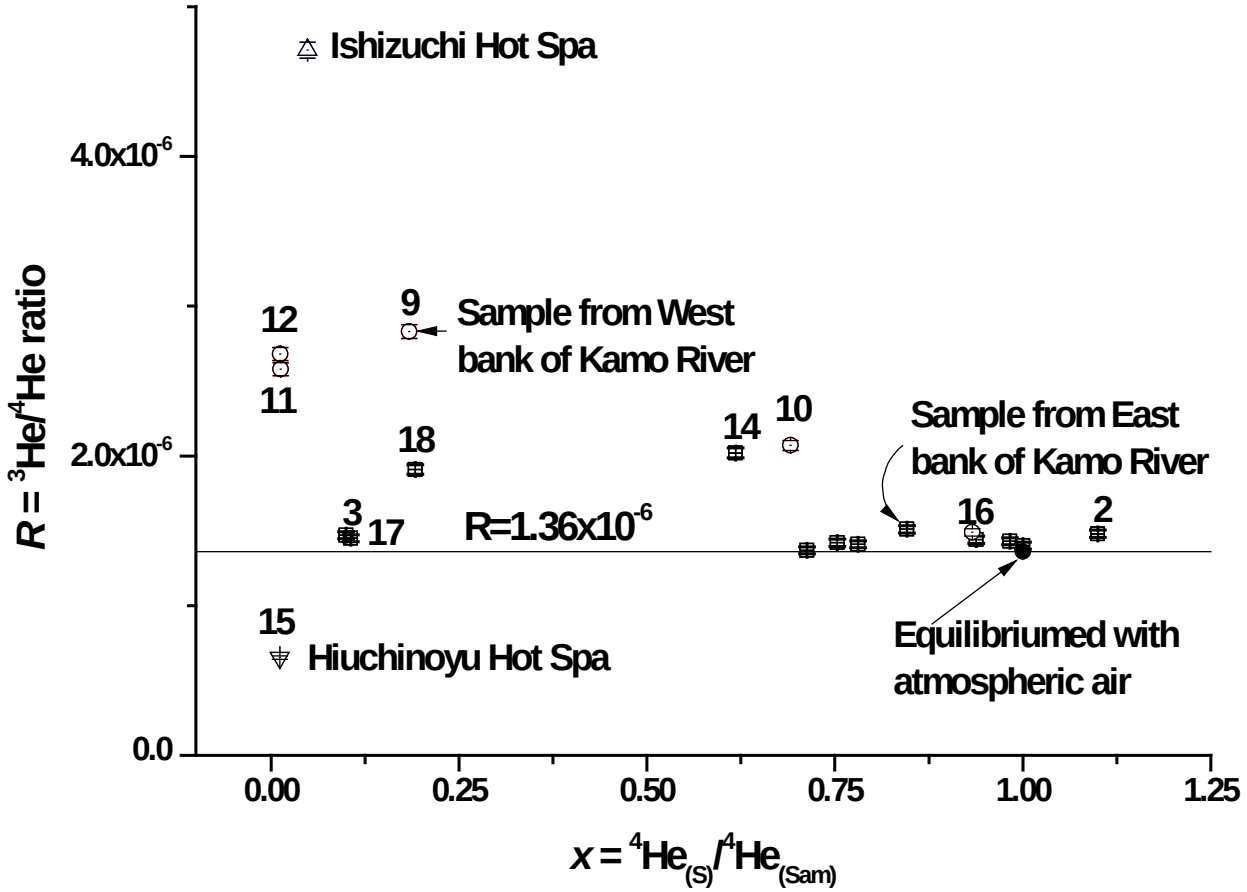
Ishizuchi Hot Spa
4.0x10-6
2.0x10-6
0.0
R = 3He/4He ratio
12
9
Sample from West
bank of Kamo River
11
14
10
Sample from East
bank of Kamo River
18
3
17
R=1.36x10-6
16
2
15
Hiuchinoyu Hot Spa
Equilibriumed with
atmospheric air
0.00
0.25
0.50
0.75
1.00
1.25
x = 4He(S)/4He(Sam)

Fig. 6

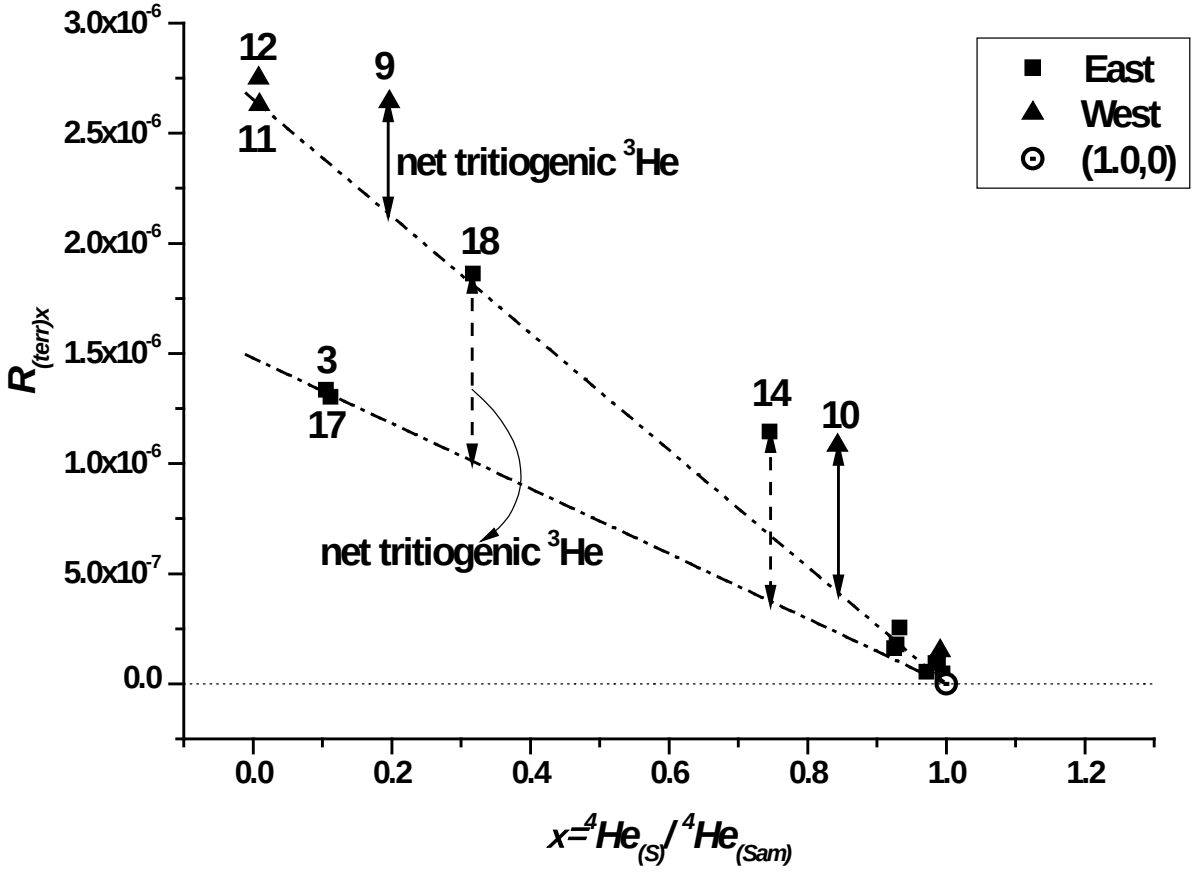
3.0x10-6
2.5x10-6
2.0x10-6
1.5x10-6
1.0x10-6
5.0x10-7
0.0
R(terr)x
0.0
0.2
0.4
0.6
0.8
1.0
1.2
x=4He(S)/4He(Sam)
East
West
(1.0,0)
12
11
9
net tritiogenic 3He
18
3
17
14
10
net tritiogenic 3He

Fig. 7

Table 1 Summary of sampling locations, sampling dates, groundwater flow zone, measurements of noble gases (He, Ne, Ar, Kr, Xe) and tritium concentration, and estimates of groundwater residence times by the proposed 3H+3He method.

Sample location	Depth (m)	Sampling date (D/M/Y)	G. W. F. Region	Measured							Estimation (excess air, temperature, saturation)				Proposed 3H+3He dating method							
				4He (cm3STP /gH2O)	R = 3He/4He	Ne (cm3STP /gH2O)	Ar (cm3ST P/gH2O)	Kr (cm3ST P/gH2O)	Xe (cm3ST P/gH2O)	Tritium (Detection limit: ± 0.25) (TU)	Initial entapped air Ae (CE-modl) (ccSTP/g)	Fractiona-tion parameter F (CE-model)	Recharge Tem-perature T (°C)	4He(S) (ccSTP/g)	4He(Sam) (cm3STP/ gH2O)	3He*(Tot) (cm3STP/gH 2O)	*X* = 4He(S) / 4He(Sam)	*R(Sam) = 3He*(Tot) / 4He(Sa*	Net of tritiogenic 3He/4He ratio (R(Sam)x − R(Terr)x) Line E	Line W	3He(tri)	Residence time: T (y)
1. Kanpusa	Seepage	15/07/2008	E	4.68E-08	1.43E-06	1.94E-07	2.83E-04	N.M.	N.M.	2.3	6.00E-04	0.36	25.0	4.41E-08	4.48E-08	4.17E-15	9.85E-01	9.31E-08	7.02E-08		3.15E-15	#######
2. Kannonsui (a)	-20	16/07/2008	E	4.32E-08	1.48E-06	2.08E-07	3.30E-04	N.M.	N.M.	3.1	7.00E-04	0.3	17.4	4.52E-08	4.07E-08	-8.90E-16	1.11E+00	#######			N.E.	
3. Minato Shinchi	-6	16/07/2008	E	4.56E-07	1.47E-06	2.55E-07	4.00E-04	N.M.	N.M.	N.D.	7.00E-03	0.42	12.5	4.60E-08	4.35E-07	5.81E-13	1.06E-01	1.33E-06			N.E.	
4. Uchinuki Hiroba (a)	-30	16/07/2008	E	5.40E-08	1.51E-06	2.04E-07	3.17E-04	N.M.	N.M.	2.4	2.30E-03	0.42	22.2	4.45E-08	4.77E-08	1.22E-14	9.33E-01	2.55E-07	1.56E-07		7.46E-15	#######
5. Modorikawa (a)	-25	16/07/2008	E	6.07E-08	1.42E-06	2.39E-07	3.87E-04	N.M.	N.M.	2.6	6.20E-03	0.42	14.6	4.56E-08	4.62E-08	4.49E-15	9.88E-01	9.74E-08	8.02E-08		3.70E-15	#######
6. Shimomachi (a)	-25	16/07/2008	E	4.87E-08	1.44E-06	1.99E-07	3.23E-04	N.M.	N.M.	2.8	2.00E-05	0.42	17.3	4.52E-08	4.86E-08	8.70E-15	9.29E-01	1.79E-07	7.39E-08		3.59E-15	#######
7. Tokumasu-tei (a)	-20	16/07/2008	E	5.85E-08	1.41E-06	2.34E-07	3.77E-04	N.M.	N.M.	2.5	3.30E-03	0.42	12.3	4.60E-08	4.97E-08	7.98E-15	9.25E-01	1.60E-07	5.01E-08		2.49E-15	#######
8. Omachi P-School	-20	17/07/2008	E	6.41E-08	1.37E-06	2.66E-07	3.78E-04	N.M.	N.M.	3.3	6.45E-03	0.36	14.8	4.56E-08	4.69E-08	2.52E-15	9.71E-01	5.38E-08	1.17E-08		5.50E-16	#######
9. Fudarakuji (a)	-45	17/07/2008	W	2.49E-07	2.83E-06	2.50E-07	4.09E-04	N.M.	N.M.	3.3	3.55E-03	0.3	9.7	4.65E-08	2.36E-07	6.25E-13	1.97E-01	2.64E-06		4.83E-07	1.14E-13	#######
10. Oshinnden (a)	-20	17/07/2008	W	6.61E-08	2.07E-06	2.39E-07	3.59E-04	N.M.	N.M.	3.0	4.20E-03	0.36	16.0	4.54E-08	5.38E-08	5.83E-14	8.43E-01	1.08E-06		6.61E-07	3.56E-14	#######
11 Igari hot-spa (a)	-60	25/12/2011	W	3.50E-06	2.58E-06	1.56E-07	2.68E-04	1.06E-07	3.00E-08	N.D.	D.G.	D.G.	8.0	4.69E-08	5.17E-06	1.36E-11	9.08E-03	2.63E-06			N.E.	
12 Yunotani hot-spa (a)	-4	25/12/2011	W	3.75E-06	2.68E-06	1.49E-07	3.41E-04	1.57E-07	5.23E-08	0.8	D.G.	D.G.	8.0	4.69E-08	5.89E-06	1.62E-11	7.97E-03	2.75E-06		7.15E-08	4.21E-13	#######
13 Kuroneko (a)	-48	26/12/2011	E	4.57E-08	1.40E-06	2.04E-07	3.90E-04	1.63E-07	5.17E-08	2.0	1.00E-05	0.75	15.5	4.55E-08	4.57E-08	2.13E-15	9.95E-01	4.65E-08	3.95E-08		1.80E-15	#######
14 Khobhosui	>-20	26/12/2011	E	7.40E-08	2.02E-06	2.44E-07	3.66E-04	1.47E-07	4.34E-08	2.3	5.00E-03	0.42	14.9	4.56E-08	6.11E-08	7.00E-14	7.46E-01	1.15E-06	7.70E-07		4.70E-14	#######
15 Hiuchi hot spa	-1005	26/12/2011	E	3.85E-06	6.53E-07	2.57E-07	4.23E-04	1.69E-07	4.74E-08	N.D.	6.80E-03	0.39	11.2	4.62E-08	3.83E-06	2.42E-12	1.21E-02	6.33E-07			N.E.	
16 Nishiizumi-higashi (a	-25	26/12/2011	W	4.90E-08	1.49E-06	2.12E-07	3.51E-04	1.45E-07	4.43E-08	0.8	8.00E-04	0.28	14.3	4.57E-08	4.61E-08	6.90E-15	9.92E-01	1.50E-07		1.27E-07	5.85E-15	#######
17 Minato Shinchi	-6	26/12/2011	E	4.30E-07	1.45E-06	2.54E-07	3.91E-04	1.51E-07	4.56E-08	N.D.	7.00E-03	0.42	13.9	4.57E-08	4.09E-07	5.33E-13	1.12E-01	1.30E-06			N.E.	
18 Kurare	-50	25/12/2011	E	2.38E-07	1.91E-06	4.06E-07	4.52E-04	1.62E-07	4.54E-08	2.3	4.80E-02	0.36	22.1	4.45E-08	1.40E-07	2.61E-13	3.17E-01	1.86E-06	8.55E-07		1.20E-13	#######

(a): Artesian flowing well
G.W.F.Region: Groundwater Flow Region. E is the east side of the Kamo river. W is the west side of the Kamo river.
N.D.: Tritium was less than the detection limits.
NE.: Not evaluation of the residence time of groundwater
N.M.: Not measure
D. G.: Degassed samples. We corrected 4He concentration and 3He/4He ratio using the diffusion model (Stute et al., 1992; Lippmann, et al. 2003) and assuming the sampling temperature of 8° C.
diffusion coefficents of D(3He) = 1.128*D(4He)
Line E and W are shown in Fig. 7, and they are mixing lines accumulated by the terrigenic He components with different 3He/4He ratio.
CE-model: Aeschbach-Herting W. et al. (2000)